A CYLINDRICAL MULTIWIRE HIGH-PRESSURE GAS PROPORTIONAL CHAMBER SURROUNDING A GASEOUS H_2 TARGET WITH A MYLAR SEPARATION FOIL 6 μm THICK⊗

U. Gastaldi*), R.D. Wendling*), E.G. Auld**), H. Averdung***), J. Bailey†), G.A. Beer**), B. Dreher***), K.L. Erdman**), E. Klempt††), K. Merle***), K. Neubecker††), C. Sabev†††), H. Schwenk††), B.L. White**) and R. Wodrich††)

ABSTRACT

The characteristics and performances of a cylindrical multiwire proportional chamber built and used at CERN in experiment S142 for the study of the $\bar{p}p$ atom spectroscopy are presented. The chamber surrounds a high-pressure gaseous H_2 target, from which it is separated by a very thin window (6 μm mylar foil). The active volume (90 cm long, 2 cm thick, internal diameter $\emptyset_I$ = 30 cm) is divided into 36 equal and independent cells each covering 10° in azimuth. At 4 abs. atm the detection efficiency for X-rays is higher than 20% in the whole energy range 1.5-15 keV. Typical resolutions are 35% FWHM for the 3 keV Ar fluorescence line and 25% FWHM for the 5.5 keV ^{54}Mn line. Working pressures from 0.5 to 16 abs. atm have been used.

Contributed paper for the
Wire Chamber Conference, Vienna, Austria,
14-16 February, 1978

⊗) Presented by U. Gastaldi.

*) CERN, Geneva, Switzerland.

**) TRIUMF, Vancouver, Canada.

***) Institut für Kernphysik, University of Mainz, Mainz, Germany.

†) Daresbury Laboratory, Warrington, Lancs, England; present address: IKO, Amsterdam, Netherlands.

††) Institut für Physik, University of Mainz, Mainz, Germany.

†††) Visitor at CERN, Geneva, Switzerland.

1. INTRODUCTION

We describe the characteristics and the performances of a cylindrical multi-wire proportional gas chamber surrounding a gaseous target, from which it is separated by a thin mylar foil.

This counter is dedicated to the detection of soft X-rays (1-15 keV) produced by exotic atoms formed by stopping negative particles ($\bar{p}$, π^-, μ^-, ...) in low Z target gases. It has good detection efficiency in the low-energy region (1-4 keV) -- where other kinds of detectors are not usable -- limited practically only by the thickness of the separation foil. The big solid-angle coverage ($\Omega/4\pi \simeq 80\%$) and the use of many independent signal wires allow the detection in coincidence of two X-rays produced in subsequent radiative transitions of one exotic atom cascade and, when stopping antiprotons, the recognition of the pattern of the subsequent annihilation through the detection of the charged prongs. The chamber can be operated in the pressure range 0-25 abs. atm to allow change of pressure in the target gas in order to study exotic atom cascades as a function of the density of the surrounding medium.

The chamber has been successfully used in an experiment at CERN which has provided the first direct observation of the formation of $\bar{p}p$ atoms[1] through the detection of the L X-ray lines (1.7-3 keV) and is at present being operated in the search for K X-ray transitions of the $\bar{p}p$ atom in the energy region 5-15 keV.

2. THE CHAMBER

2.1 Physical constraints on the design

The main constraints imposed on the chamber design by the physics are listed below.

i) The sensitive volume of the chamber has to extend up to the foil separating it from the target volume in order to avoid a dead region. The counter gas contained in the dead region would filter the X-rays transmitted by the foil with a transmission efficiency depending on the pressure and on the X-ray energy and angle of incidence. This pressure-dependent window effect would make the treatment of low-energy X-ray data hardly manageable.

ii) The separation foil has to be as thin as possible in order to allow a reasonable transmission (> 10%) for X-rays with energy below 3 keV, but thick enough to prevent appreciable diffusion of the target gas in the counter region (this changes the working conditions of the proportional counter) and of the counter gas in the target region (this causes uncontrolled X-ray absorption in the target region and transfer processes in the exotic atoms).

iii) The separation foil must have a good cylindrical shape with constant diameter and no wrinkles, as its surface acts as a cathode for the multiwire chamber. The position of the foil has to be stable in order to avoid changes in the gain and in the X-ray detection efficiency.

2.2 Design principles

The design principles adapted to match the physical constraints illustrated above were then as follows:

i) the separation foil had to be kept at ground potential in order to act as the internal cathode surface of the chamber;

ii) the target and counter gases had to be flushed;

iii) the separation foil had to be exchangeable without having to disassemble any other parts of the chamber;

iv) the pressure difference across the separation foil had to be stabilized actively.

2.3 Mechanical construction

The general layout of the chamber is illustrated schematically in Fig. 1. The active volume is a 90 cm long toroid ($\emptyset_i$ = 30 cm, $\emptyset_o$ = 34 cm), delimited outside by a grid set at ground potential (100 μm copper wire, 3 mm spacing, winding parallel to the chamber axis) and inside by a mylar tube ($\emptyset$ = 30 cm) aluminized on the external surface and set at the same ground potential as the grid. The external grid and the mylar tube are the cathodes of the chamber. Thirty-six anode wires (20 μm gold-coated tungsten), stretched parallel to the chamber axis at 10°

from each other at a radius of 16 cm, divide the active volume into 36 independent equal cells. The cells are separated from each other by 36 intermediate wires (100 μm copper) installed at 16 cm radius alternatively with the anode wires.

Anode and intermediate wires are kept at constant tension by springs. The mylar membrane is kept in position by two expansion rings pressing, via an ungreased O-ring, the mylar tube at its two extremities against the frame of the chamber. This pressure ensures both the gas tightness between the target and chamber region and a good grounding of the aluminized surface of the mylar.

The frame of the counter (Figs. 2 and 3) consists of two anticorodal rings (supporting the wires, the grid, and the mylar tube) connected at the exterior of the active volume by spacing bars made of thin stainless-steel tube.

The anode and intermediate wires, and the external cathode grid, are installed once and for all on the frame with no membrane present. The whole system is quite rigid, but rather light so that it can be handled easily by one person alone during the operations of insertion and extraction of the mylar tube. A detailed description of the chamber construction and of the technique for the insertion of the mylar membrane is presented elsewhere[2].

2.4 Chamber installation

The chamber is surrounded inside the pressure vessel by 36 plastic scintillator slabs put in one to one correspondence with the 36 chamber cells. It encloses a sophisticated system of plastic scintillation counters, which are mounted at the two extremities of the chamber and are used to select the particles of the beam which stop in the target gas.

The chamber axis is aligned with the beam line. The distance between the chamber and the wall of the 36 surrounding scintillators is very little in order to minimize the volume of chamber gas. A description of the complete apparatus will be given in a forthcoming paper[3].

2.5 Gas handling

Both the counter gas and the target gas are flushed to minimize the content of impurities coming from degassing of the scintillators and diffusion through the mylar membrane. The flushing rates are of the order of 1 ℓ min^{-1} at normal temperature and pressure (NTP).

An overpressure of $\Delta p \approx 1$ Torr on the side of the target gas makes the mylar tube become an almost perfect cylinder. The overpressure Δp is stabilized within the limits $\delta(\Delta p) = \pm 0.1$ Torr by an active gas regulation system[3]: variations of the pressure difference within these limits cause expansions ($\delta p > 0$) and compressions ($\delta p < 0$) of the membrane, hardly appreciable by looking at it and do not affect noticeably the energy gain.

The pressure difference Δp is controlled independently of the vessel pressure and maintained within safety limits: 0 Torr $< \Delta p <$ 3 Torr during filling and emptying operations. The membrane survives, however, overpressures of 10 Torr. 25 μ, 12 μ, and 6 μ thick aluminized mylar membranes have been used.

3. THE ELECTRONICS

The proportional chamber is exposed to a high flux of charged particles, as the beam energy degrader is installed inside the chamber itself. This imposes, for the electronics of the proportional counter, the use of a good pulse-shape discrimination in order to be able to distinguish between pulses produced by X-rays and pulses due to charged particles.

An X-ray absorbed in the chamber gives a pulse with short rise-time, as the energy deposition is highly localized, while a charged particle traversing the chamber ionizes more or less uniformly along its path and the primary electrons drift for different times before reaching the anode wire, causing a long rise-time of the pulse.

The rise-time information is stored for every pulse and the pulse-shape discrimination is applied off line.

3.1 High-voltage distribution

The aluminized mylar cathode and the external cathode grid are grounded together with the frame of the chamber and the stainless-steel vessel. The positive high voltage (HV) is distributed to the anode wires through a distribution network illustrated in Fig. 4. A spark plug is used as a HV vacuum high-pressure feedthrough and the 10 MΩ resistors decouple the anode signals from each other. The HV decoupling capacitors on the anode wires are installed inside the vessel in the counter gas region to avoid noise from the vacuum high-pressure feedthroughs.

The intermediate wires alternating with the anode wires are biased to a negative HV of the order of 1/10 of the positive HV applied to the anodes, to provide a clearing field and a better separation between contiguous cells. The negative HV is distributed by a busbar without decoupling resistors.

3.2 Signal processing

The signals from the anode wire of one cell of the chamber are treated completely independently from those of the other cells. The block diagram of the electronics attached to each cell is given in Fig. 5. The charge preamplifier is connected directly to the high-pressure signal feedthrough. The gain of each postamplifier is variable in order to equalize the gain of the 36 independent channels. The output (B) of the amplifier fires a discriminator which stops a time-to-digital converter (TDC) and triggers two gate generators. The TDC measures the drift-time of the pulse; the gate generators open two charge-sensitive ADCs ("A" and "C"). The data are, event by event, transferred via CAMAC to a HP 21MX minicomputer, which preprocesses and stores the data on magnetic tape.

The outputs A and C of the amplifier give equal signals. The two gates a and c start at the same time, but have different widths (a = 180 nsec, c = 450 nsec). The contents of the two ADCs "A" and "C" are therefore only equal if the recorded pulses are not longer than 180 nsec. X-ray pulses are shorter than 100 nsec, whereas pulses of charged particles extend typically for more than 250 nsec, causing different readings of the ADCs "A" and "C".

The pulse-shape discrimination is made off line, applying a suitable cut for the quotient of the content of the ADCs "A" and "C". The quotient cut is defined experimentally using X-ray sources.

4. PERFORMANCES

The chamber has been pressurized up to 25 abs. atm during measurements of the rate of stops of beam particles in the target gas.

The behaviour of the chamber as a proportional counter has been tested up to 16 abs. atm using Ar + 5%C_3H_8 counter gas, H_2 target gas, and a 6 μm mylar foil. Table 1 shows the pressure dependence of the HV necessary to provide a constant gain and that of the FWHM energy resolution for 5.5 keV X-rays from a ^{54}Mn source.

The in-beam behaviour is strongly dependent on the pressure (for a given gain), owing to the variation of the total energy loss for charged particles traversing the chamber. The optimization of the a and c gate lengths for the pulse-shape discrimination has been done at 4 abs. atm with the standard filling (Ar + 5% C_3H_8 counter gas, H_2 target gas). The counter has been operated mostly at 4 abs. atm; data were also collected at 1.1 and 8 abs. atm; typical operating conditions with non-standard gas mixtures are listed in Table 2.

In the following we refer, unless otherwise explicitly stated, to the standard filling at 4 abs. atm. In-beam conditions were studied at the m_{14} 900 MeV/c anti-proton beam of the CERN Proton Synchrotron with typically 2000 $\bar{p}$'s/burst for 2×10^{11} p's on the internal production target, 10/1 $\pi^-/\bar{p}$ contamination, and 250 msec long slow ejection.

4.1 Energy calibration

4.1.1 Generalities

For the absolute energy calibration we used the nominal peaks and the associated escape peaks of X-ray sources, and the 3 keV X-rays of the beam-induced Ar fluorescence lines (Table 3). The sources were located in the centre of the plastic scintillator at the downstream end of the chamber, which is used as a veto counter for the beam stop definition (see Fig. 1).

With this source geometry, and adding off-line the signals of all the wires the typical energy resolution for 5.5 keV ^{54}Mn X-rays is $\sim$ 25% at FWHM. Particularly good cells have 20% resolution.

For this position of the source, the calibration measurements test essentially the behaviour of the downstream half of the chamber. The stability of the gain and of the resolution along the wires was checked, sliding and rotating a collimated source along the chamber axis: under well-controlled conditions of the mylar foil (Δp = 1 Torr, δp = $\pm$0.1 Torr) the gain of every cell is stable within $\pm$5% and the resolution does not change appreciably. Moreover the Ar fluorescence 3 keV X-rays allow a calibration with rather uniform illumination of the whole chamber. In the analysis we accept the signal from a cell only if the two adjacent cells on both sides did not fire. This way we use only fluorescence X-rays, which escape the cell where they are produced and traverse the target region by crossing twice the mylar foil. This minimizes the risk of adding to the X-ray signals the signals of δ-rays from charged particles traversing the borders of the cell. The typical resolution for the 3 keV Ar fluorescence peak is 35% at FWHM, in agreement with the measurements taken with the sliding source.

4.1.2 Beam-on beam-off comparison

When the chamber is exposed to the beam the gain reduces, owing to the drop of the potential of the anodes caused by the current drawn through the 10 MΩ decoupling and protecting resistors. The average total current through the chamber is of the order of 1 μA in typical beam conditions. The change of gain depends on the HV setting and on the beam intensity and can be as high as 10%. After the first 50 msec of beam spill the gain remains stable within a few per cent for a flat beam spill. Gating off the first 50 msec of beam spill at each burst the resolution is as good as in beam-off conditions.

A calibration line in the same in-beam conditions as the data spectrum is necessary to account for the gain changes due to fluctuations of the beam intensity.

4.1.3 Calibration trigger

The 835 keV γ-ray of the ^{54}Mn source, emitted in coincidence with the X-ray, is able to fire the supporting scintillator, thus providing a prompt trigger signal. The γ-trigger is vetoed by any beam particle. A γ-triggered calibration goes on in parallel with data taking and allows the use of a very weak source. We used a 160 nCi ^{54}Mn source during all data-taking runs; the source peak does not appear in the stop-triggered data. The ^{54}Mn source has, moreover, the advantage that the 5.5 keV line is far in energy from the expected position of both the L and K X-ray lines of the $\bar{p}p$ atom.

4.1.4 Linearity

The linearity of the response of the chamber and of the electronics was measured between 2.5 and 14.4 keV in beam-off conditions, adding to the 160 nCi ^{54}Mn source a 500 nCi ^{57}Co source and using the γ-triggered mode to select the ^{54}Mn signals out of the 6.5 keV ^{57}Co dominant contribution.

The in-beam linearity is permanently monitored between 3 and 5.5 keV, using the 3 keV Ar fluorescence line and the γ-triggered 5.5 keV line of the ^{54}Mn. The zero-energy points of the beam-on and beam-off linearity curves are in good agreement (Fig. 6). The beam-on linearity was in addition checked up to 14 keV, by using N_2 gas in the target region and detecting $6 \rightarrow 5$ $\bar{p}N$ X-ray transitions and down to 1.8 keV, by filling the target region with He and detecting $5 \rightarrow 4$ $\bar{p}$He transitions.

4.2 Detection efficiency

The X-ray transmission of the mylar window for various thicknesses and normal incidence is plotted in Fig. 7 versus the X-ray energy.

For a given mylar thickness the detection efficiency depends on the composition and on the density of the counter gas and on the spatial distribution of the beam particles stopping in the target gas. The stopping efficiencies of some of the counter gas mixtures employed are plotted versus the X-ray energy for NTP conditions and normal incidence (2 cm thick active region) in Fig. 8. In Fig. 9 is

shown the detection efficiency of the proportional chamber for normal incidence in the conditions where most of the $\bar{p}p$ data were collected. Within statistics, the measured detection efficiency is the same for all the 36 cells of the chamber.

The absence of dead regions in the chamber has been checked at the 15% level with two independent measurements: a) by measuring the ratio between the number of 5.5 keV ^{54}Mn X-rays detected in the γ-triggered mode and the number of γ triggers (this measurement is independent of the activity of the source); b) by comparing the nominal activity of the source with the total number of X-rays detected in a known interval of time.

4.3 Drift-time measurements

For the drift-time measurements, a common start to all 36 TDCs is given by the $\bar{p}$-stop signal for data events and by the γ trigger for the calibration events; the stop of every TDC is given by the discriminator of the corresponding cell.

Soft X-rays coming from the target region are absorbed in the chamber preferentially near the mylar foil, while the stop distribution of the more energetic ones is more uniform.

This results in a longer average drift-time for low-energy X-rays: the exploitation of this information allows a better background rejection.

The effect of drift-time dependence on the X-ray energy has been simulated and observed by comparing the drift-time spectra of the 5.5 keV line taken at various pressures with constant gas gain (Fig. 10).

The drift-time information proved to be very useful, because the gain depends slightly on the drift-time. Knowing this dependence from source measurements, it was possible to improve substantially the over-all resolution.

4.4 Pulse-shape discrimination

The great improvement in the identification of the X-ray pulses, resulting from the application of the pulse-shape discrimination, is evident when comparing in-beam X-ray spectra with the appropriate rise-time cut, with the spectra where

the cut is not applied. This comparison is made in Fig. 11 for a γ-triggered source spectrum and in Fig. 12 for a data spectrum taken in the standard conditions at 4 abs. atm.

In Fig. 13 is shown a peak of X-rays of the L lines of the $\bar{p}p$ atom, obtained by applying the usual rise-time cut and requiring that only one cell of the 36 of the chamber had fired (this requirement imposes a selection on the $\bar{p}p$ annihilation pattern and suppresses the Ar fluorescence contamination). For comparison, the Ar fluorescence calibration peak, obtained from the same set of the data, is also shown.

5. CONCLUSIONS

The chamber has been operating satisfactorily for more than one year, and the reliability of the technique of installing and exchanging the membrane has been proved by many changes of the mylar foil, made to optimize the high X-ray transparency/low gas diffusion compromise, without any bad effect on the wires.

When comparing with the proportional counter used in a previous apparatus[6] that allowed the detection of the first X-rays from H_2 and D_2 exotic atoms, the biggest advantages are: a) $\sim$ 100 times bigger solid-angle coverage; b) the possibility of detecting in coincidence two X-rays of the same atomic cascade. This has made necessary a much more sophisticated mechanical construction[2] and a gas-regulation system with two orders of magnitude higher accuracy.

Considering the reliability of the present chamber, a development allowing a complete spatial localization of the incident X-ray (or charged particle) seems conceivable by using a thin mylar membrane with a printed pattern of conducting strips perpendicular to the anode wires and acting as a cathode. A high spatial accuracy in the axial direction could be obtained by the determination of the charge centroid of the pulses induced on the cathode strips[7].

Such a counter could be the core of a 4π detection apparatus intended to study the $\bar{p}p$ annihilation in detail (with the signature of the quantum numbers of some of the atomic levels from which the annihilation occurs) when a low-momentum ($p < 400$ MeV/c) cooled ($\Delta p/p < 10^{-3}$) $\bar{p}$ beam will be available[8]. Considering

that a cooled $\bar{p}$ beam would have no pion contamination and could have an $\sim$ 100% macroscopic duty cycle and that, in the present situation ($p \approx 900$ MeV/c, $\Delta p/p > 1\%$ before moderation), the bulk of charged particles crossing the chamber comes from $\bar{p}$ annihilation in the beam degrader and in the scintillators surrounding the chamber, an improvement of the effective $\bar{p}$ stop rate in the target of a factor of 10^4 is conceivable and could be handled by the present electronics.

Acknowledgements

We should like to acknowledge the support of the CERN EP Division and Dr. E. Picasso, in particular, for his encouragement.

We also wish to thank Mr. F. Jeanmairet for the accurate machining of all the chamber components, Mr. G. Sicher for technical advice and support, Messrs. C. Deillon and H. Bresson for their help in the assembling of the mylar tube stretcher.

REFERENCES

1) E.G. Auld, H. Averdung, J. Bailey, G.A. Beer, B. Dreher, H. Drumm, K.L. Erdman, U. Gastaldi, E. Klempt, K. Merle, K. Neubecker, C. Sabev, H. Schwenk, R.D. Wendling, B.L. White and R. Wodrich, to be submitted to Phys. Letters.

2) U. Gastaldi, Design, construction and conceivable developments of a cylindrical multiwire high-pressure proportional chamber with ultrathin cylindrical internal window, CERN EP Internal Report in preparation.

3) E.G. Auld, H. Averdung, J. Bailey, G.A. Beer, B. Dreher, K.L. Erdman, U. Gastaldi, E. Klempt, K. Merle, K. Neubecker, C. Sabev, H. Schwenk, R.D. Wendling, B.L. White and R. Wodrich, to be submitted to Nuclear Instrum. Methods.

4) J. Legrand, J.P. Perolat, F. Lagoustine and Y. le Gallic, Table de Radionucléides, LMRI, CEA (1975).

5) E. Storm and H.L. Israel, Academic Press, Inc., Nuclear Data Tables A7 (1970) 565.

6) A. Placci, E. Polacco, E. Zavattini, K. Ziock, G. Carboni, A. Di Bene, U. Gastaldi, G. Gorini, G. Neri and G. Torelli, Nuclear Instrum. Methods 91 (1971) 417.

7) A. Breskin, G. Charpak, C. Demierre, S. Majewski, E. Policaro, F. Sauli and J.C. Santiard, Nuclear Instrum. Methods 143 (1977) 29 and references quoted therein.
See also G. Charpak, G. Petersen, A. Policarpo and F. Sauli, Progress in high-accuracy proportional chambers, to be published in Nuclear Instrum. Methods.

8) See, for example, U. Gastaldi, A possible new experimental approach to the study of the $\bar{p}p$ system at low energies *in* Exotic Atoms, Proc. First Internat. School of Physics of Exotic Atoms, Erice 24-30 April 1977, Italy (eds. G. Fiorentini and G. Torelli) Servizio Documentazione dei Laboratori di Frascati, December 1977, and references quoted therein.

Table 1

HV and energy resolution dependence on pressure for constant gain.
Standard gas mixture (95%Ar + 5%C_3H_8), 6 μm mylar.

p (abs. atm)	0.5	1.1	4	8	12	16
HV (V)	900	1300	2450	3500	4250	5000
FWHM energy resolution at 5.5 keV (%)	26	27	25	24	27	30

Table 2

Typical operating conditions with non-standard gas mixtures

Counter gas	Pressure (abs. atm)	HV (V)	FWHM energy resolution at 5.5 keV (%)	Maximum drift-time for 5.5 keV X-rays (μsec)
80% CO_2^+ 20% CH_4	4	5200	32	5
90% Ne^+ 10% C_2H_6	8	3450	29	2

Table 3

X-ray sources used for calibration.
Data on radioactive sources are from Ref. 4

X-ray source	Transition	Absolute yield per disintegration (%)	Energy (keV)	Average energy (keV)
$\bar{p}$He	5 → 4			1.8
Ar fluorescence	K			3
^{54}Mn	K_α	22.8	5.41	5.5
	K_β	2.7	5.96	
	Escape peak	Pressure dependent		2.5
^{57}Co	K_α	49.2	6.40	6.5
	K_β	6.6	7.08	
	Escape peak	Pressure dependent		3.5
	γ	9.6	14.4	14.4
$\bar{p}$N	6 → 5			14

Figure captions

Fig. 1 : General layout of the proportional chamber. The plastic scintillators surrounding the Cu energy degrader and the proportional chamber have not been drawn for sake of clarity.

Fig. 2 : Chamber frame. The frame is deposited on top of a mylar tube prepared on its assembling tool and ready for insertion.

Fig. 3 : Cylindrical multiwire proportional chamber

Fig. 4 : HV and signal connections of the anode wires. The resistors and capacitors indicated in the drawing are installed inside the vessel in the counter gas region.

Fig. 5 : Block diagram of the electronics of one channel of the multiwire chamber. The gates on the two ADCs of one cell are opened only if the discriminator associated with that cell fired. The start signal of the TDCs is common for all cells.

Fig. 6 : Calibration of the energy response of the multiwire chamber. The beam-on points are obtained with beam intensity higher than the standard one.

Fig. 7 : X-ray transmission of the mylar foil for normal incidence. The photon cross-sections tabulated in Ref. 5 have been used for the computation.

Fig. 8 : X-ray absorption in 2 cm of counter gas. The absorption in the quenching gas has been taken into account.

Fig. 9 : X-ray detection efficiency of the proportional chamber. Calculation for 12 μ thick mylar foil, 4 abs. atm standard filling and normal incidence. The maximum detection efficiency for incidence at 30° to the mylar foil surface is also shown.

Fig. 10 : Drift-time spectra of the 5.5 keV line. The spectra were taken at several pressures in the proportional chamber, with 6 μm mylar and standard counter gas, adjusting the HV when changing pressure so as to keep the gas gain constant.

Fig. 11 : In-beam γ-triggered spectrum of the ^{54}Mn source: in (a) no rise-time cut is applied, in (b) the rise-time cut providing the best signal-to-noise ratio is applied.

Fig. 12 : Data spectrum. In (a) no rise-time cut is applied; in (b) the same rise-time cut as in Fig. 11b is applied. The peak at 3 keV is due to the Ar fluorescence. One sees that the pulse-shape discrimination is most effective at X-ray energies comparable to the minimum ionization loss of charged particles crossing the chamber.

Fig. 13 : $\bar{p}p$ atom L X-ray spectrum. For comparison, the Ar fluorescence spectrum, obtained from the same set of data with a different trigger, but with the same rise-time cut, is also shown.

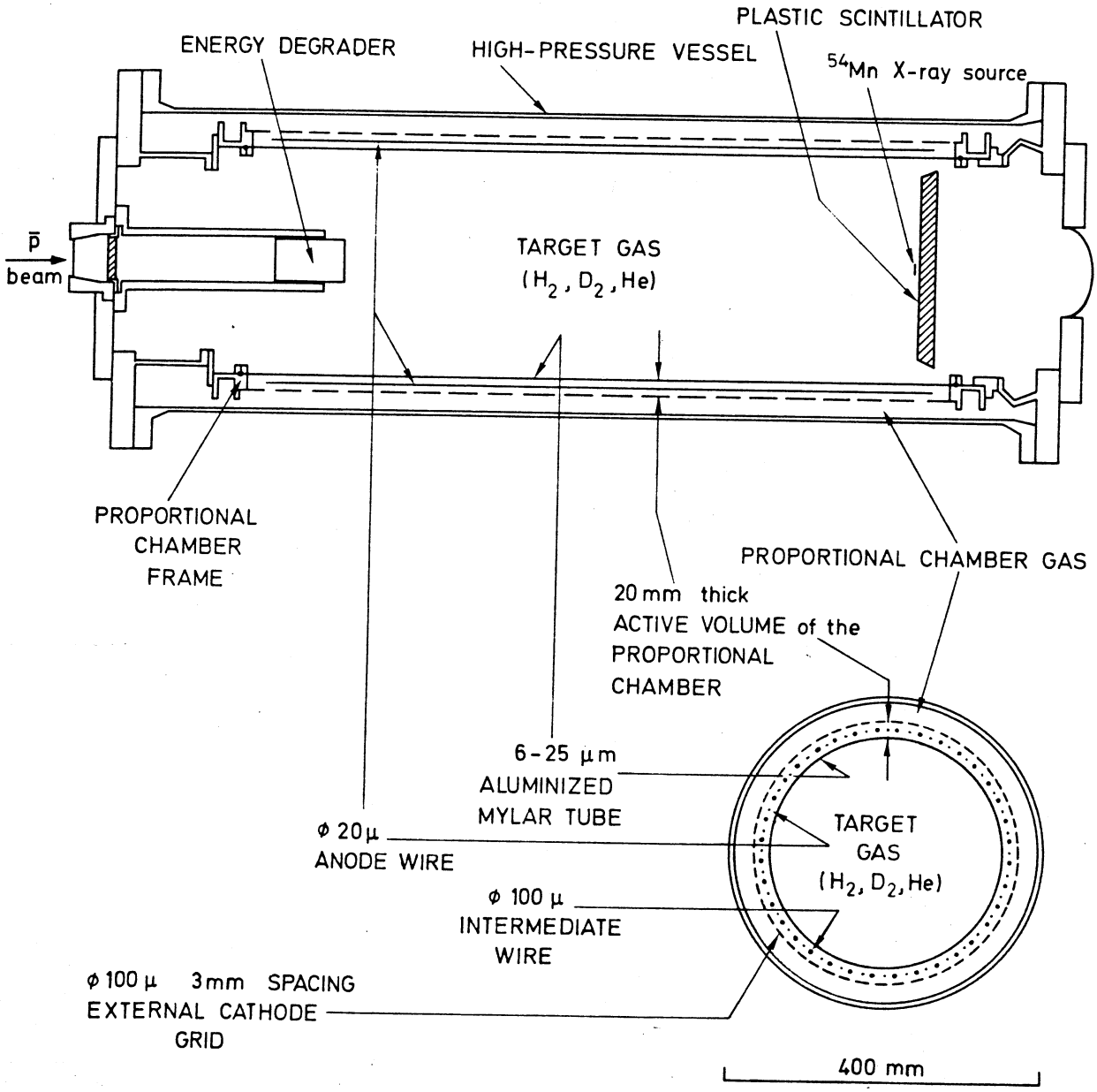
PLASTIC SCINTILLATOR
ENERGY DEGRADER
HIGH-PRESSURE VESSEL
^{54}Mn X-ray source
$\bar{p}$ beam
TARGET GAS (H_2, D_2, He)
PROPORTIONAL CHAMBER FRAME
PROPORTIONAL CHAMBER GAS
20 mm thick ACTIVE VOLUME of the PROPORTIONAL CHAMBER
6-25 μm ALUMINIZED MYLAR TUBE
φ 20μ ANODE WIRE
TARGET GAS (H_2, D_2, He)
φ 100 μ INTERMEDIATE WIRE
φ 100 μ 3mm SPACING EXTERNAL CATHODE GRID
400 mm

Fig. 1

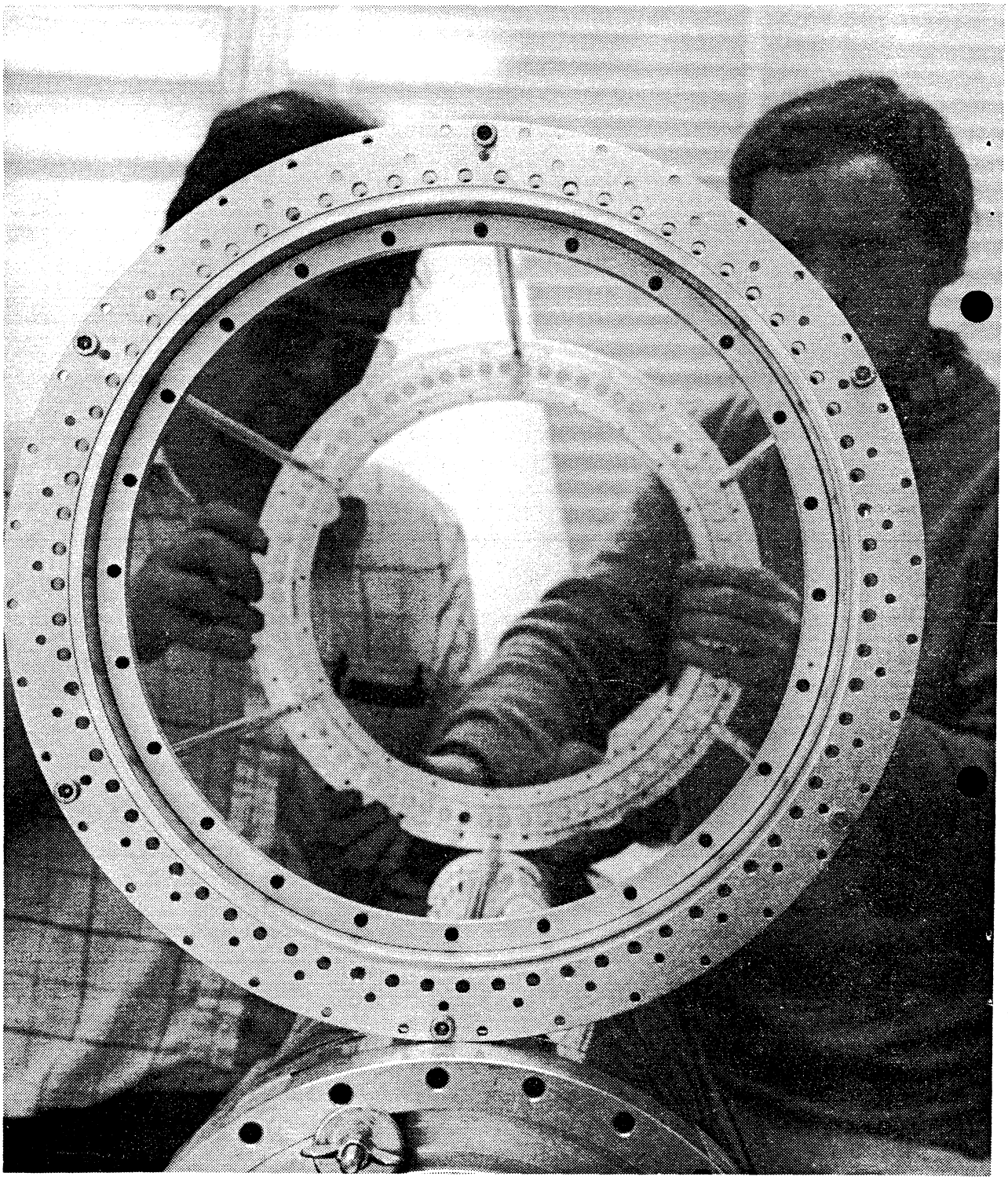

Fig. 2

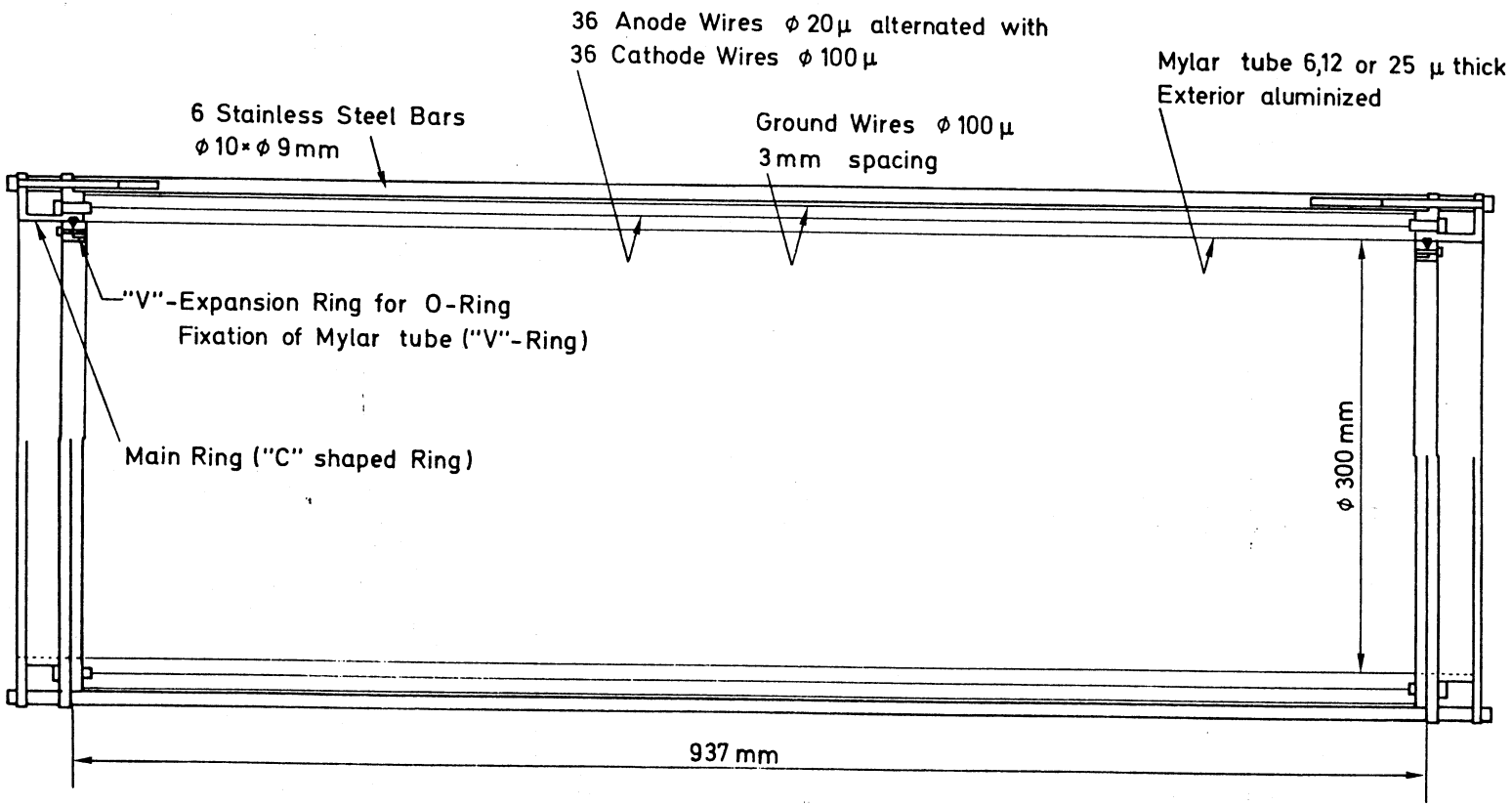
36 Anode Wires ϕ 20 μ alternated with
36 Cathode Wires ϕ 100 μ
Mylar tube 6,12 or 25 μ thick
Exterior aluminized
6 Stainless Steel Bars
ϕ 10 × ϕ 9 mm
Ground Wires ϕ 100 μ
3 mm spacing
"V"-Expansion Ring for O-Ring
Fixation of Mylar tube ("V"-Ring)
Main Ring ("C" shaped Ring)
ϕ 300 mm
937 mm

Fig. 3

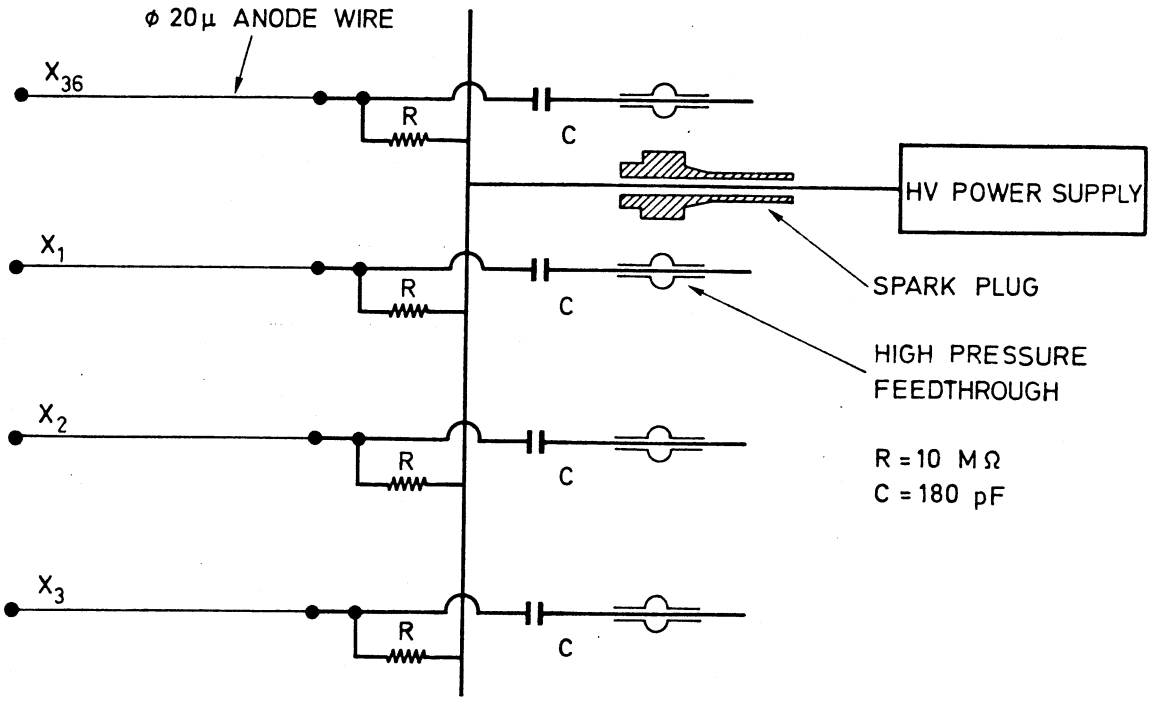
φ 20μ ANODE WIRE
X36
X1
X2
X3
R
C
HV POWER SUPPLY
SPARK PLUG
HIGH PRESSURE
FEEDTHROUGH
R = 10 MΩ
C = 180 pF

Fig. 4

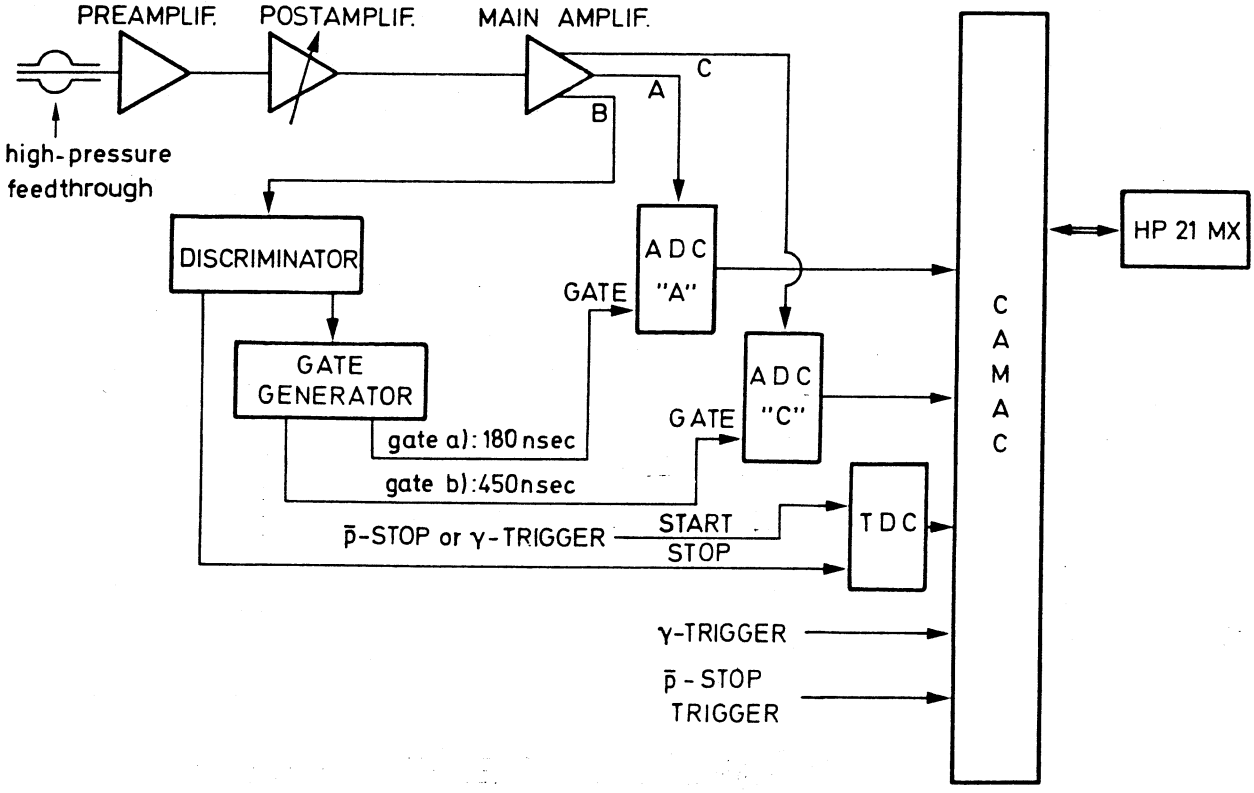
PREAMPLIF.
POSTAMPLIF.
MAIN AMPLIF.
high-pressure
feedthrough
A
B
C
DISCRIMINATOR
GATE
GENERATOR
ADC
"A"
ADC
"C"
GATE
GATE
gate a): 180 nsec
gate b): 450 nsec
p̄-STOP or γ-TRIGGER
START
STOP
TDC
γ-TRIGGER
p̄ - STOP
TRIGGER
CAMAC
HP 21 MX

Fig. 5

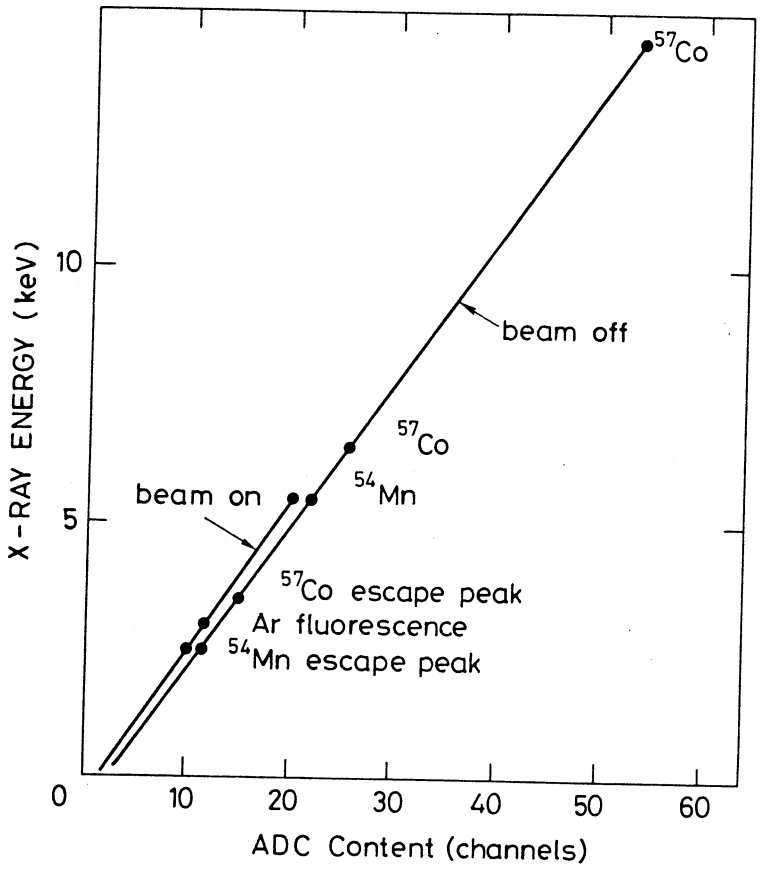
X-RAY ENERGY (keV)
ADC Content (channels)
0
5
10
10
20
30
40
50
60
^{57}Co
beam off
^{57}Co
^{54}Mn
beam on
^{57}Co escape peak
Ar fluorescence
^{54}Mn escape peak

Fig. 6

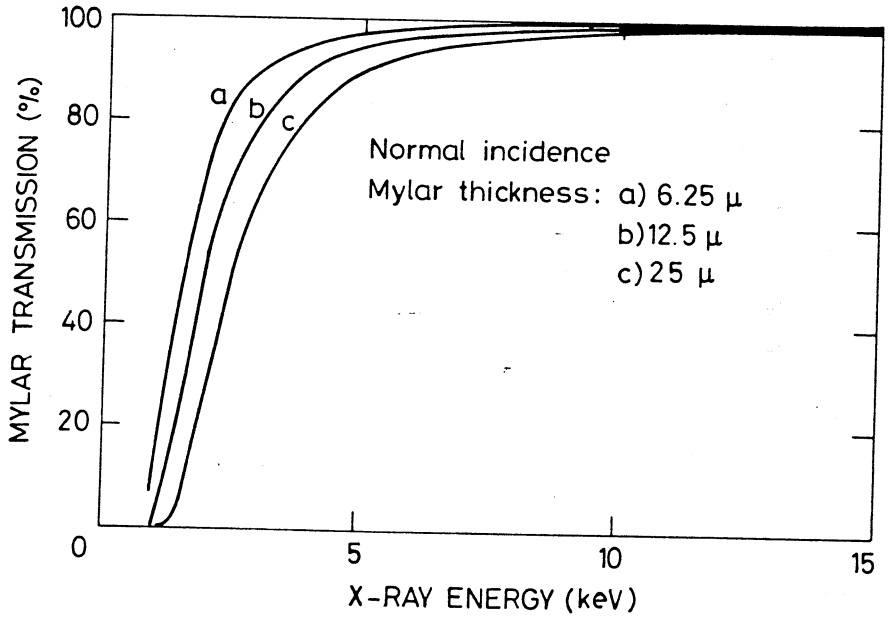
MYLAR TRANSMISSION (%)
X-RAY ENERGY (keV)
0
20
40
60
80
100
5
10
15
a
b
c
Normal incidence
Mylar thickness: a) 6.25 μ
b) 12.5 μ
c) 25 μ

Fig. 7

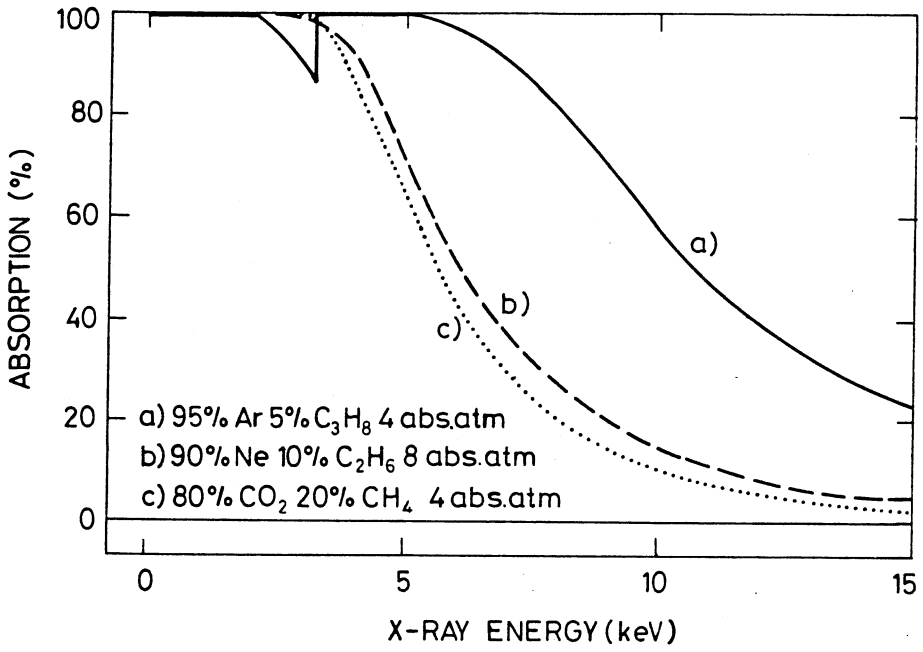
ABSORPTION (%)
100
80
60
40
20
0
0
5
10
15
X-RAY ENERGY (keV)
a)
b)
c)
a) 95% Ar 5% C_3H_8 4 abs.atm
b) 90% Ne 10% C_2H_6 8 abs.atm
c) 80% CO_2 20% CH_4 4 abs.atm

Fig. 8

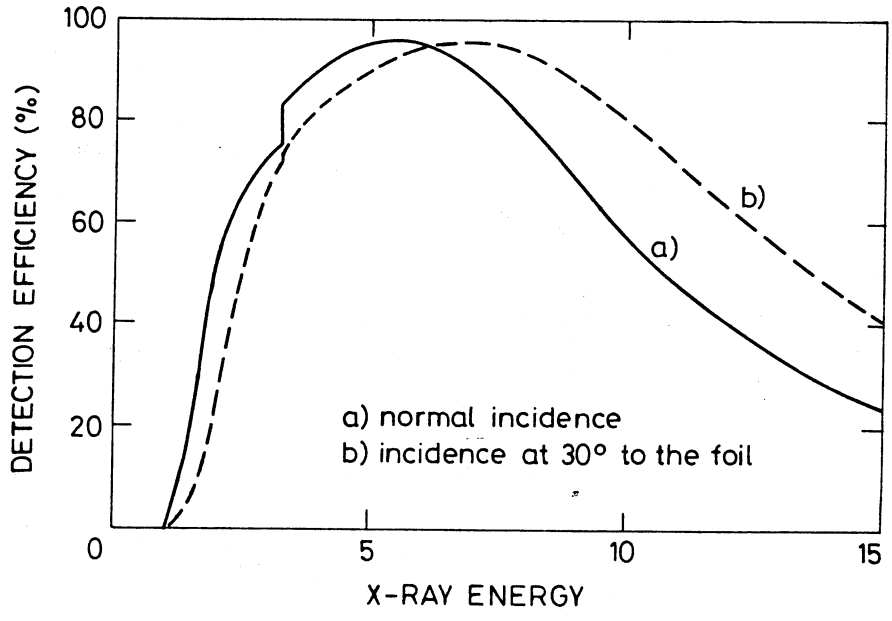
DETECTION EFFICIENCY (%)
100
80
60
40
20
0
5
10
15
X-RAY ENERGY
a)
b)
a) normal incidence
b) incidence at 30° to the foil

Fig. 9

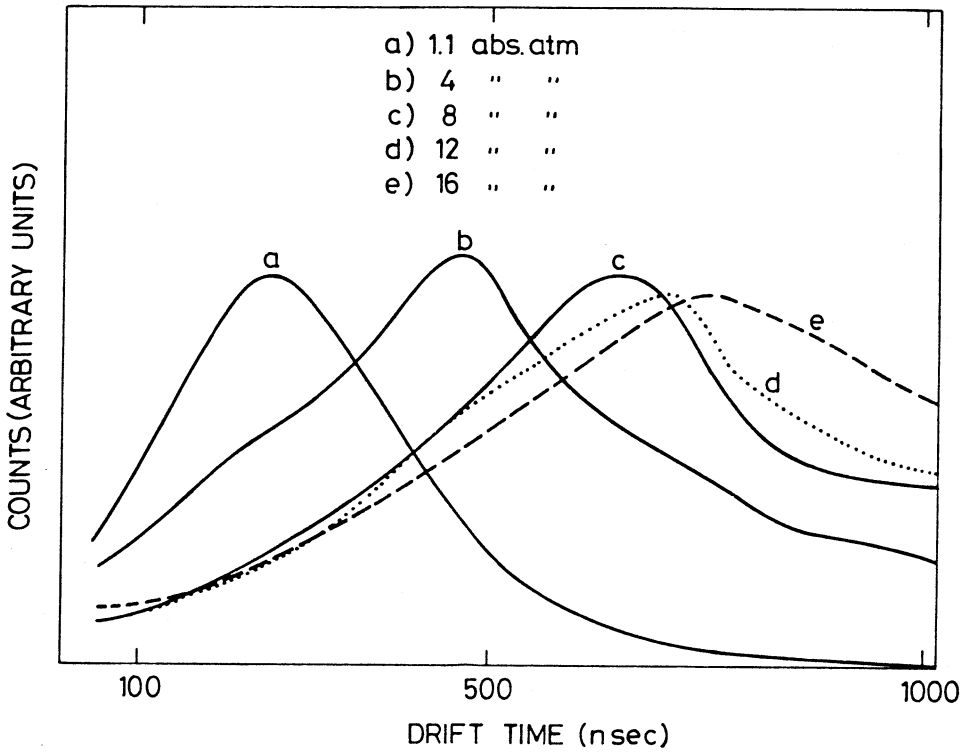
a) 1.1 abs. atm
b) 4 " "
c) 8 " "
d) 12 " "
e) 16 " "
a
b
c
d
e
COUNTS (ARBITRARY UNITS)
100
500
1000
DRIFT TIME (n sec)

Fig. 10

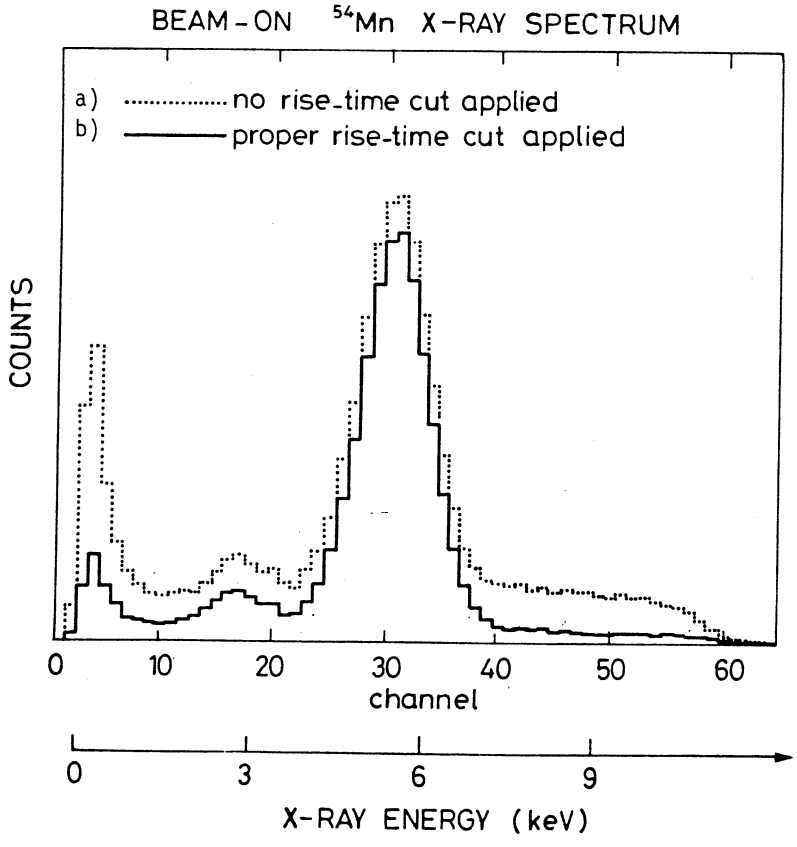
BEAM - ON ^{54}Mn X-RAY SPECTRUM
a) ..... no rise-time cut applied
b) ——— proper rise-time cut applied
COUNTS
0
10
20
30
40
50
60
channel
0
3
6
9
X-RAY ENERGY (keV)

Fig. 11

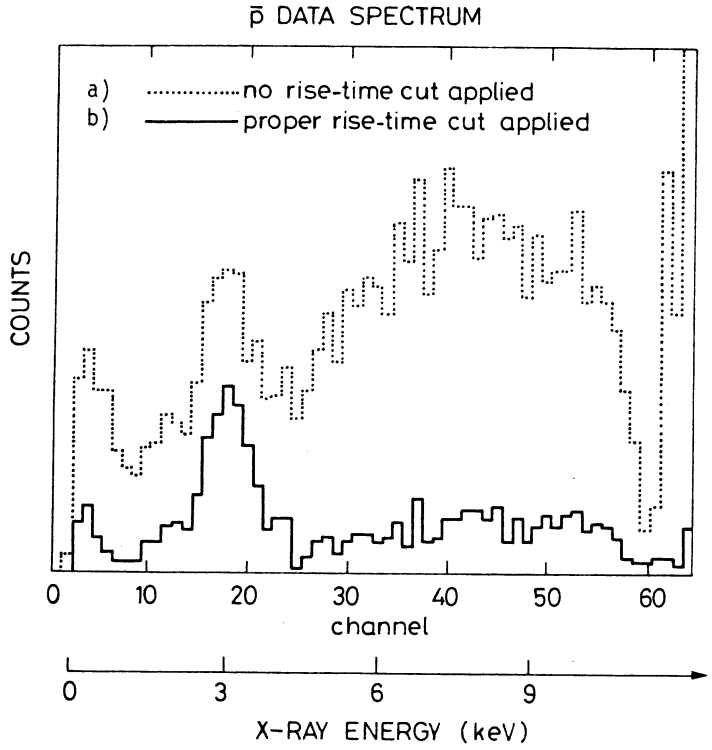
p̄ DATA SPECTRUM
a) ..... no rise-time cut applied
b) ——— proper rise-time cut applied
COUNTS
0
10
20
30
40
50
60
channel
0
3
6
9
X-RAY ENERGY (keV)

Fig. 12

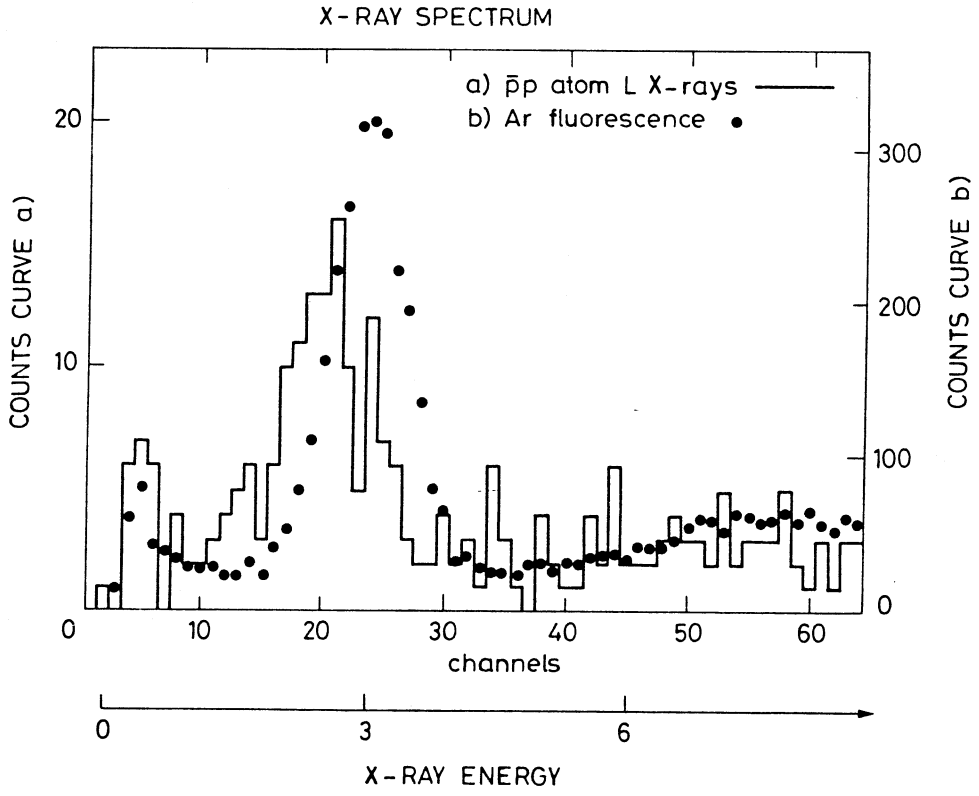
X-RAY SPECTRUM
a) p̄p atom L X-rays
b) Ar fluorescence
COUNTS CURVE a)
COUNTS CURVE b)
20
10
0
300
200
100
0
10
20
30
40
50
60
channels
0
3
6
X-RAY ENERGY

Fig. 13